JOURNAL OF MATERIALS SCIENCE 28 (1993) 553–560

The effects of hydroxide gel drying on the characteristics of co-precipitated zirconia–hafnia powders

H. P. LI, J. WANG *, R. STEVENS
School of Materials, The University of Leeds, Leeds, LS2 9JT, UK

Mixed zirconia–hafnia ($Hf_{0.25}Zr_{0.75}O_2$) powders of fine particle size and narrow particle-size distribution can be prepared via co-precipitation routes using mixed zirconium and hafnium salts as the starting materials. The characteristics of the resultant zirconia–hafnia powders are dependent strongly on the dehydration route by which the co-precipitated hydroxide gels are dried. Zirconium–hafnium hydroxide gels are formed when zirconium and hafnium oxynitrates are co-precipitated in an ammonia solution of pH 10.5. The co-precipitated hydrous gels were dried by three very different routes including organic solvent dehydration, microwave drying, and conventional infrared heating lamp drying. The dried hydroxides were then calcined at various temperatures in the temperature range 550–1150 °C, followed by ball milling to remove large soft-particle agglomerates. The resultant zirconia–hafnia powders were characterized for crystallite size, particle size, particle-size distribution, particle morphology, and the degree of powder agglomeration, using experimental techniques such as X-ray diffraction, BET surface area, differential thermal analysis, thermo-gravimetric analysis, sedigraph, scanning and transmission electron microscopy. Hard particle aggregates, which cannot be effectively eliminated using ball milling, occur in the zirconia–hafnia powders processed via either the microwave drying or conventional infrared heating lamp drying routes. In contrast, the organic solvent dehydration route resulted in an almost aggregate-free powder of fine crystallite and particle sizes. Therefore, the zirconia–hafnia powder processed via the organic solvent dehydration route exhibited high sinterability on sintering at 1300 °C.

1. Introduction

Transformation toughening has recently been well established in zirconia-dispersed ceramics, following the discovery of stress-induced transformation toughening in the mid-1970s [1]. However, zirconia-toughened ceramics do not exhibit desirable mechanical properties at elevated temperatures, simply as a result of the low monoclinic to tetragonal transformation temperature occurring in zirconia [2, 3]. Although hafnia has widely been suggested as a potential substitute for zirconia for high-temperature applications, high-temperature toughening has not been well demonstrated in hafnia-dispersed ceramics [4, 5]. It is technically difficult to retain the metastable tetragonal hafnia phase in a ceramic matrix, as the critical particle size for the spontaneous tetragonal to monoclinic transformation in monolithic hafnia is in the range 5–10 nm [6, 7]. Owing to their strikingly similar crystal structures and phase transformations, hafnia and zirconia form a continuous solid solution over the entire range of composition [8]. The physical characteristics of a zirconia–hafnia solid solution, such as the monoclinic to tetragonal transformation temperature and the critical particle size for the spontaneous tetragonal to monoclinic transformation, are dependent on its composition. Specifically, all these parameters obey approximately the rule of mixture. Naturally, zirconia–hafnia solid solution is a technologically important toughening agent for engineering applications in the intermediate temperature range. The zirconia–hafnia solid solution should have a smaller inclusion size than monolithic zirconia, in order to retain the metastable tetragonal phase in a sintered ceramic matrix. It is therefore essential to have a zirconia–hafnia powder of fine particle size and narrow particle-size distribution as the starting material for these transformation-toughened ceramics, capable of giving toughness at intermediate temperatures.

Co-precipitation is one of the most commonly used methods for producing undoped and doped zirconia and hafnia powders of fine particle size and narrow particle-size distribution [9, 10]. Hydroxide gels are formed when zirconium or hafnium salt solutions, such as nitrate and chloride, are added to an ammonia solution. The subsequent drying and calcination of the co-precipitated hydroxide gels lead to the formation of

Present address: IRC in Materials for High Performance Applications, The University of Birmingham, Birmingham, B15 2TT, UK

0022–2461

undoped and doped zirconia and hafnia powders. This involves the dehydration, crystallization of amorphous zirconia or hafnia and the subsequent crystal growth, together with possible particle agglomeration when the co-precipitated hydroxide gels are dried and calcined. An appropriate drying route is of paramount importance, in order to avoid undesirable crystal growth and the formation of powder agglomerates. Zirconia or hafnia powders with a coarse crystallite size and a high degree of powder agglomeration exhibit a low sinterability and therefore a high sintering temperature [11]. Furthermore, it may be thermodynamically impossible to retain the metastable tetragonal phase in a sintered ceramic matrix, when the grain size of a zirconia–hafnia solid solution is large enough, i.e. above the critical particle size for the spontaneous tetragonal to monoclinic transformation on cooling from the sintering temperature. Ideally, the dehydration of co-precipitated hydrous oxide gels is completed at temperatures as low as possible. Freeze drying is a good example which demonstrates the fact that ceramic powders dried at low temperatures exhibit a minimum degree of hard agglomeration and therefore a high degree of sinterability at relatively low sintering temperature [12]. However, the low production efficiency of the freeze drying technique largely limits its application on an industrial scale.

In comparison, conventional heat drying of ceramic powders is simple and of low cost. However, hard powder agglomerates or aggregates may form in a conventionally heat-dried ceramic powder. Microwave drying has advantages such as speed, high-energy efficiency, and a uniform moisture distribution in the dried powders [13, 14]. Organic solvent dehydration of hydrous oxides does not involve a significantly high temperature. It is therefore attractive in terms of avoiding the formation of any hard particle agglomerates in the dried powders [15, 16]. The aim of the present work was to investigate the impact of various drying routes on the characteristics of co-precipitated zirconia–hafnia powders.

2. Experimental procedure

The composition of $Hf_{0.25}Zr_{0.75}O_2$ was chosen for this work on the consideration that the critical particle size for the spontaneous tetragonal to monoclinic transformation in this composition is in the range 50–100 nm. The sintering of a nanosized $Hf_{0.25}Zr_{0.75}O_2$ powder at temperatures below 1300 °C may result in a grain size which is comparable to the critical particle size and therefore a dense crack-free ceramic body. Fig. 1 shows the experimental procedure followed in the present work. Zirconium oxynitrate solution and hafnium oxynitrate powder, or hafnyl nitrate, were used as the starting materials. Table I lists the chemical analysis for the as-received zirconium oxynitrate solution and hafnium oxynitrate powder. Appropriate amounts of zirconium oxynitrate solution and hafnium oxynitrate powder were calculated on the basis of the desired composition and then mixed together in distilled water to obtain a 0.1 M salt solution. Co-precipitation was carried out by dropping the mixed oxynitrate salt solution from a Burette pipette to an aqueous ammonia solution of pH 10.5, while the ammonia solution was being vigorously stirred. The co-precipitated gel suspension was aged for 24 h. The hydroxide gels were then filtered out from the aqueous suspension, followed by repeated water washes, until the nitrate ions in the washing solution reached a trace level.

The water-washed hydroxide gels were dried using three different routes, namely organic solvent dehydration using acetone and toluene, microwave drying, and conventional infrared heat drying. These three approaches are referred as OR, MW, and IR, respectively, in the following discussions. For the OR drying, the hydrous oxide cake was repeatedly acetone washed four times, followed by toluene and then acetone

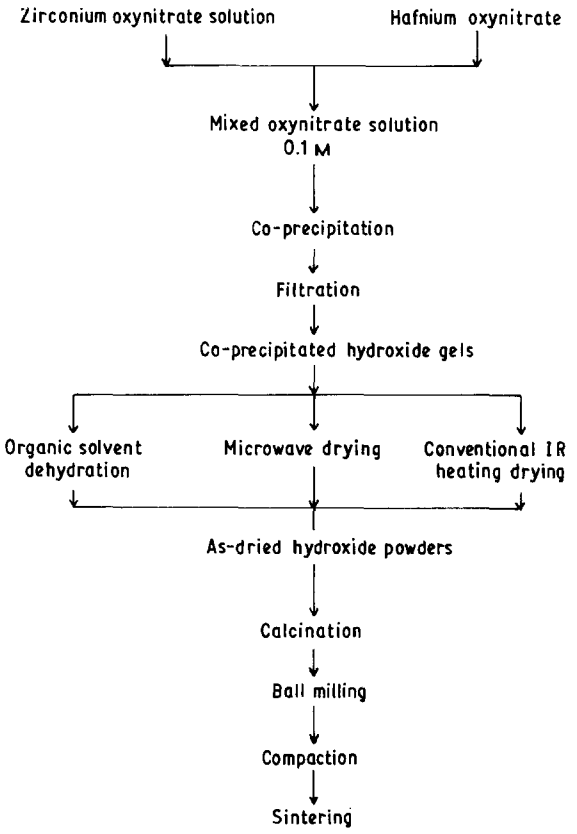

Figure 1 A diagram showing the experimental procedure followed in this work.

TABLE I The chemical analysis of the as-received zirconium oxynitrate solution and hafnium oxynitrate powder from Magnesium Elektron Ltd, Twickenham, UK and Teledyne Wah Chang, Alabany, USA, respectively

	$ZrO(NO_3)_2 x\ H_2O$	$HfO(NO_3)_2 2H_2O$
ZrO_2	19.6 wt %	0.91 wt %
HfO_2	0.4 wt %	53.5 wt %
SiO_2	< 100 p.p.m.	< 50 p.p.m.
Al	n/a	< 35 p.p.m.
Cu	n/a	< 20 p.p.m.
Fe	100 p.p.m.	50 p.p.m.
Na	< 100 p.p.m.	n/a
Ti	n/a	< 25 p.p.m.
Zn	n/a	< 50 p.p.m.

washes, to dehydrate the hydroxide gels. The organic solvent-washed cake was then kept in a vacuum flask for 24 h to evaporate off the residual organic solvents. In the MW route, the hydrous oxide cake was dried at temperatures of 80–100 °C in a commercially available Sharp 430 microwave oven which generates 650 W outpower at 2450 MHz at a 5.5 A input current, until the weight loss in a 5 min interval was negligible. For the conventional IR drying, the hydrous oxide cake was dried at temperatures of 50–70 °C under an IR heating lamp till the weight loss was negligible.

The dried hydroxide powders were then calcined for 4 h in air at various temperatures in the temperature range 550–1150 °C at a heating rate of 3 °C min^{-1}. Ball milling in ethanol for 4 h using zirconia balls as milling media was used to eliminate large soft agglomerates in the calcined powders, prior to uniaxial compaction at 50 MPa followed by isostatic pressing at 200 MPa. The isostatically pressed powder compacts were finally fired at temperatures in the range 1300–1550 °C for 2 h using heating and cooling rates of 10 °C min^{-1}.

The characteristics of both the as-dried hydroxide and ball-milled oxide powders in various stages described above are monitored using X-ray diffraction (XRD) for phase identification, BET for specific surface area, differential thermal analysis (DTA) and thermogravimetric analysis (TGA) for thermal behaviour, sedigraph, scanning and transmission electron microscopies for particle size and particle morphology.

3. Results and discussion

It was shown by XRD phase analysis that all three as-dried hydrous oxides were amorphous. However, the drying route had a dramatic effect on the particle/aggregate size and particle/aggregate morphology, and the degree of particle agglomeration in the as-dried hydrous oxides. Fig. 2a–c are scanning electron micrographs showing the particle/aggregate size and particle/aggregate morphology of the as-dried hydrous oxides processed via OR, MW and IR routes, respectively. The organic solvent dehydrated hydroxide powder exhibits a fine particle size, together with a limited amount of soft powder agglomerates. By contrast the microwave-dried hydroxide powder consists of particle agglomerates ranging from 2–10 μm in size. The hydroxide particles of the conventional IR heating dried powder are highly aggregated together, forming large angular agglomerates ranging from 5–20 μm in size. The difference in particle/aggregate morphology and in the degree of particle agglomeration among these three hydroxide powders was further observed using transmission electron microscopy (TEM), as shown in Fig. 3a–c. As was indicated by selected-area diffraction (SAD), all three as-dried hydrous oxides were amorphous. This agrees well with the experimental results of XRD phase analysis. The hydroxide agglomerates exhibit an angular morphology for the microwave dried powder and a flake-like morphology for the conventional IR heating dried powder.

The low degree of powder agglomeration in the organic solvent dehydrated hydroxide powder is also shown by BET specific surface area measurement. Table II lists the BET specific surface area values and the equivalent particle sizes for both hydroxides and oxides processed via the OR, MW and IR routes. The organic solvent dehydrated hydroxide powder exhibits a BET surface area of 208.9 $m^2 g^{-1}$, which almost doubles the BET surface area for either the microwave dried or conventional heat-dried hydroxide powders. The low degree of hydroxide agglomeration in the organic solvent dehydrated powder led to an increase in specific surface area and therefore a decrease in particle and crystallite sizes in the calcined and then ball-milled oxide powder. As was indicated by XRD phase analysis, a calcination at 600 °C for 4 h resulted in complete dehydration of the zirconium–hafnium hydroxides and therefore the formation of $Hf_{0.25}Zr_{0.75}O_2$ powder. Specifically, the calcination is a combined process of dehydration, nucleation and the subsequent crystal growth of $Hf_{0.25}Zr_{0.75}O_2$ powder particles. There is a fall in

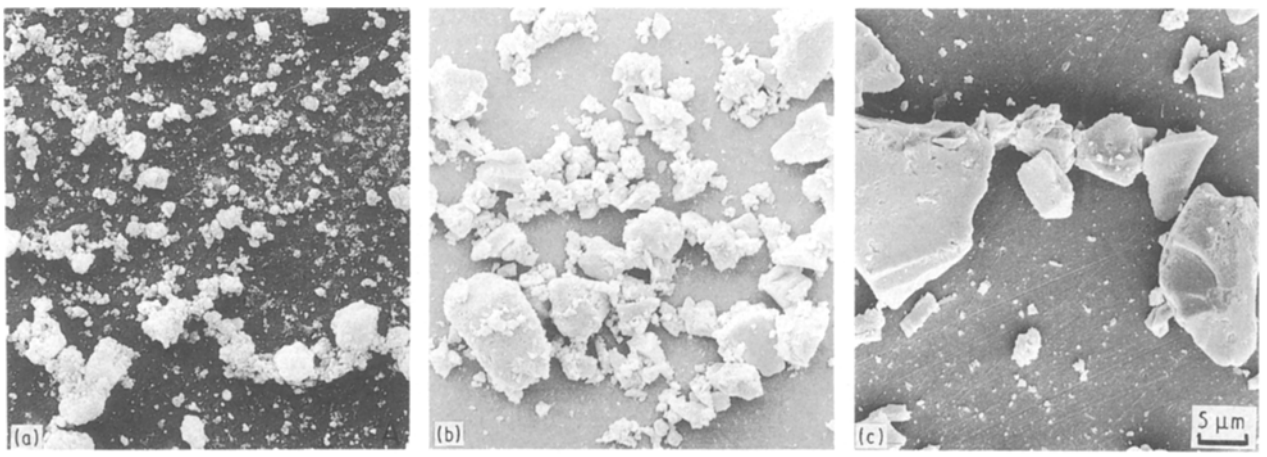

Figure 2 Scanning electron micrographs showing the particle/aggregate size, particle/aggregate-size distribution, and the degree of particle agglomeration in the as-dried hydroxides processed via (a) organic solvent dehydration, (b) microwave drying, and (c) conventional IR heating lamp drying routes.

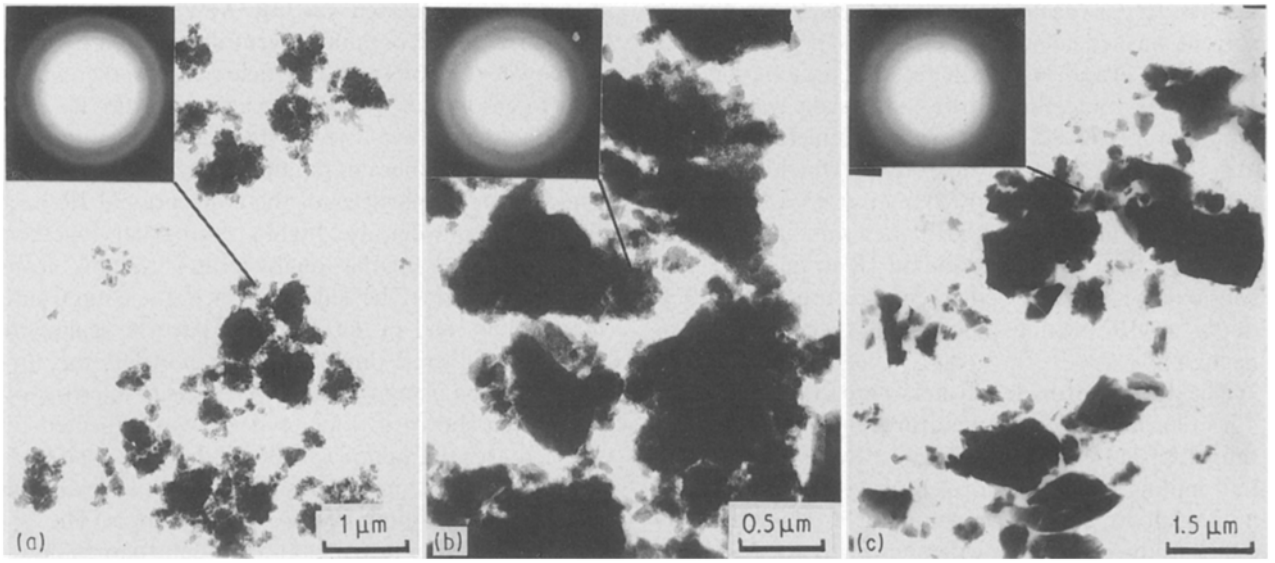

Figure 3 Bright-field transmission electron micrographs and the associated SAD patterns for the as-dried hydroxide powders processed via (a) organic solvent dehydration, (b) microwave drying, and (c) conventional IR heating lamp drying routes.

TABLE II BET specific surface areas and the equivalent particle sizes for the as-dried hydroxides and the calcined and then ball-milled oxides processed via organic solvent dehydration, microwave drying, and conventional heating lamp drying route, respectively

Drying route	BET surface area ($m^2 g^{-1}$)		Crystallite size of calcined oxide (nm)
	Hydrous oxide	Oxide	
OR	208.9	33.1	26.4
MW	112.4	26.4	33.0
IR	110.3	23.9	36.5

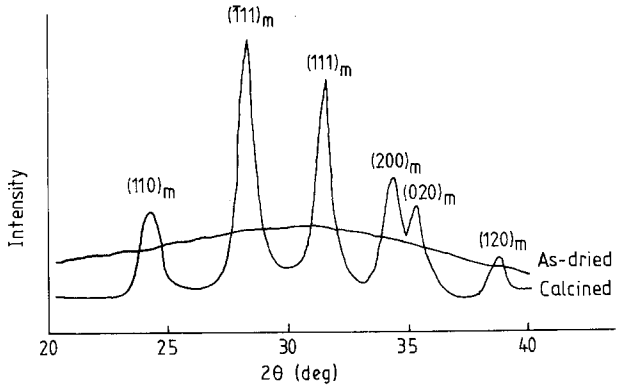

Figure 4 XRD traces for both the organic solvent dehydrated hydrous $Hf_{0.25}Zr_{0.75}O_2$ oxide and the oxide calcined at 600 °C for 4 h.

BET specific surface area and a large rise in average particle and crystallite sizes when a hydrous oxide is calcined at an appropriate temperature. Fig. 4 shows that monoclinic phase was the only phase present in the $Hf_{0.25}Zr_{0.75}O_2$ oxide processed via the organic solvent dehydration (OR) route on completing calcination at 600 °C for 4 h. This is in agreement with the experimental work performed by Tau *et al.* [17], who observed 100% monoclinic phase in the co-precipitated $Hf_{0.25}Zr_{0.75}O_2$ powder and showed that up to 100% tetragonal phase could be retained in monolithic zirconia powders prepared via the identical precipitation route when the pH value of the supernatant liquid was controlled in certain ranges. Apparently, the retention of the metastable tetragonal phase in monolithic zirconia is due to the fact that it exhibits a smaller critical particle size for the spontaneous tetragonal to monoclinic transformation than the hafnia-alloyed zirconia.

The secondary particle-size distributions in the calcined and then ball-milled $Hf_{0.25}Zr_{0.75}O_2$ powders prepared via the three different drying routes are shown in Fig. 5. These results may not truly represent the particle-size distribution in each powder, as certain powder agglomerates might not be properly dispersed during the process of sample preparation for sedigraph measurement. Therefore, the average particle size in each powder may be smaller than the particle size shown in Fig. 5. However, these particle-size distributions do indicate the average degree of powder agglomeration in the co-precipitated zirconia–hafnia powders. The powder processed via the IR route exhibits a larger average particle/aggregate size and a wider particle-size distribution than the powder processed via either the MW route or the OR route. The powder processed via the OR route exhibits the finest average particle/aggregate size. For example, the average particle size is 1.3, 1.5 and 6.0 μm for the powders processed via the OR, MW and IR drying routes, respectively.

It was observed using SEM and TEM that the

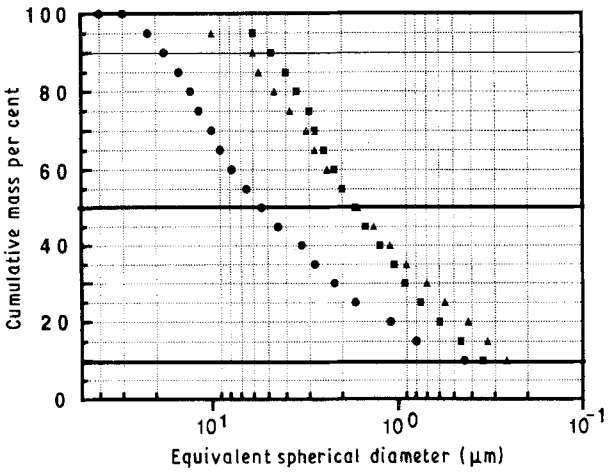

Figure 5 The secondary particle/aggregate-size distributions measured using sedigraph in $Hf_{0.25}Zr_{0.75}O_2$ powders processed via three different drying routes. The organic solvent dehydration dried oxide powder exhibits the finest average particle size. (▲) OR, (■) MW, (●) IR.

primary particle or crystallite size and the degree of powder agglomeration vary significantly in the oxide powders processed via different drying routes, as shown in Figs. 6a–c and 7a–c. The calcined and then ball-milled oxide powder processed from the hydroxide dried via the OR route exhibits a lower degree of powder agglomeration and a much smaller average particle size than the powder processed from the hydroxide dried via either the MW route or the IR route. It consists of particle agglomerates of 1–5 μm in size, and its primary particle sizes are in the range 0.1–0.2 μm, which is comparable with its average crystallite size. The oxide powder processed from the hydroxide dried via the MW route consists of both small powder agglomerates of submicrometre-sized primary particles and intermediate particle aggregates of 1–4 μm in size, which are angular in morphology, although it exhibits a submicrometre-sized average crystallite size. The secondary particle/aggregate sizes of the conventional IR heating dried oxide powder are

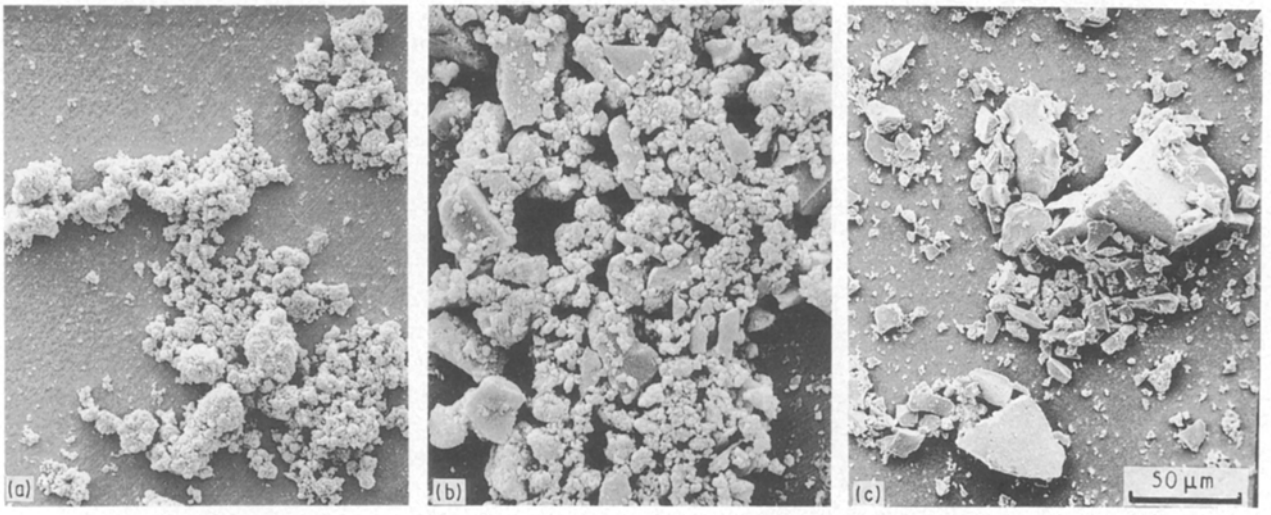

Figure 6 Scanning electron micrographs showing the calcined and then ball milled oxide powders processed via (a) organic solvent dehydration, (b) microwave drying, and (c) conventional heating drying routes.

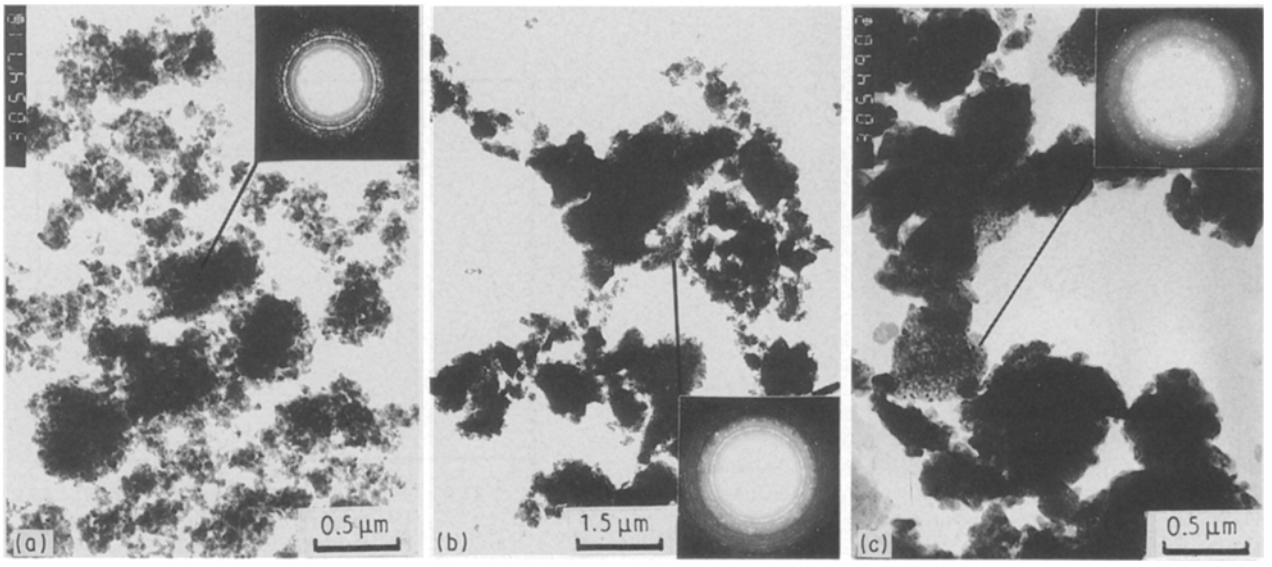

Figure 7 Bright-field transmission electron micrographs and the associated SAD patterns for the calcined and then ball-milled oxide powders processed via (a) organic solvent dehydration, (b) microwave drying, and (c) conventional heating drying routes.

in the range 3–8 μm. These particles/aggregates, which exhibit a flake-like morphology, were fractured from even larger hard powder aggregates when they were ball milled. They exhibit a much more angular morphology than the organic solvent dehydrated oxide powder, together with clearly visible fracture surfaces.

Fig. 8a–c are three bright-field transmission electron micrographs further showing the crystallite and primary particle sizes within particle agglomerates for the three powders processed via different drying routes. The powder processed from the hydroxide dried via the OR route consists of almost uniformly sized individual oxide crystals of 30–50 nm in size. Some of these microcrystals are well dispersed and the others form soft powder agglomerates. Visible bonding between individual crystals is not seen. In the oxide powder processed from the hydroxide dried via the MW route, however, neck bonding is clearly seen between these individual submicrometre-sized crystals, implying that a degree of diffusion had taken place on completing calcination at 600 °C for 4 h. In the powder processed from the hydroxide dried via the IR route, the individual $Hf_{0.25}Zr_{0.75}O_2$ crystals are also strongly aggregated together by a visible diffusion bonding neck, forming hard particle aggregates, although their average crystallite size is not much larger than that in the powder processed via the OR route. By comparing Figs 6a–c, 7a–c, and 8a–c with Figs 2a–c and 3a–c, it is clear that the occurrence of large particle aggregates in the powders processed via the MW and IR routes is due to the high degree of hydroxide agglomeration in the corresponding hydroxides. The low degree of particle aggregation in the organic solvent dehydrated oxide powder is due to the well-dispersed state in the as-dried hydroxide precursor.

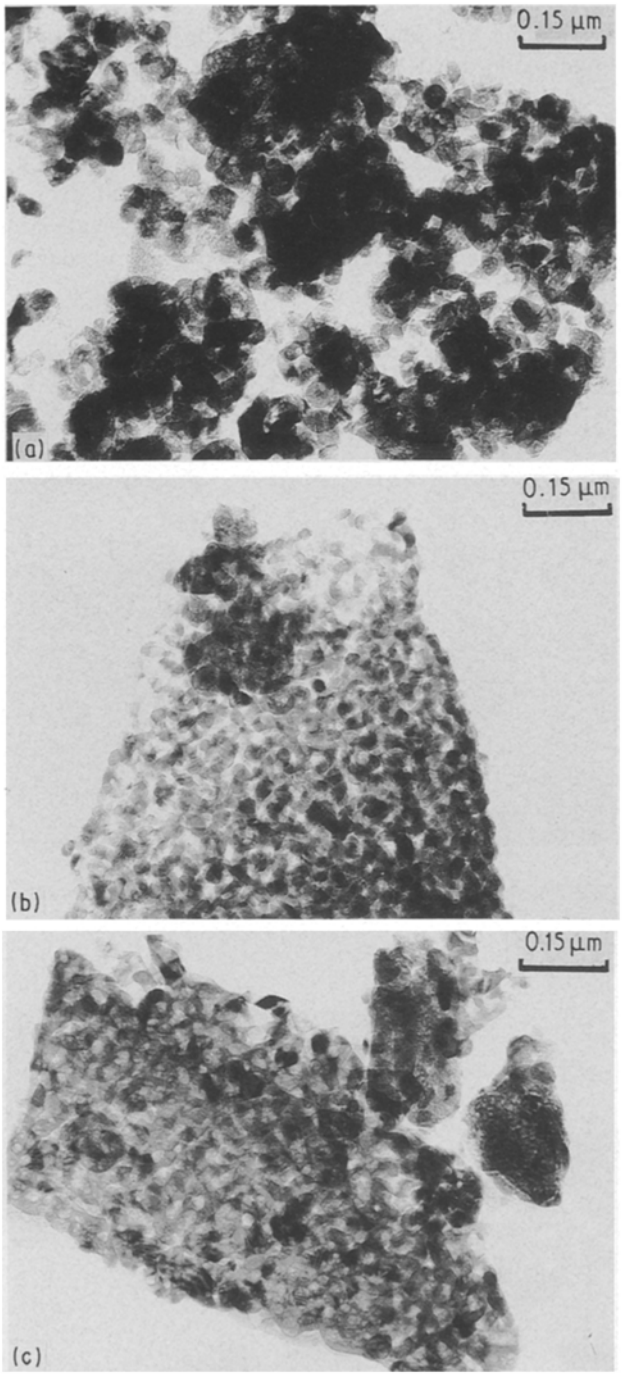

Figure 8 Bright-field transmission electron micrographs showing the internal structure of particle agglomerates for the $Hf_{0.25}Zr_{0.75}O_2$ powders processed via (a) organic solvent dehydration, (b) microwave drying, and (c) conventional heating drying routes. The submicrometre crystals are loosely agglomerated in the organic solvent dehydrated oxide powder. However, a strong aggregation of submicrometre-sized $Hf_{0.25}Zr_{0.75}O_2$ crystals is observed both in the microwave-dried and in the conventional heating lamp-dried oxide powders.

It was demonstrated by both DTA and TGA studies that the thermal behaviour of the as-dried hydrous oxides is dependent on the drying route, as is shown in Figs 9 and 10. Weight loss of 15–20 wt % occurred in the temperature range 50–300 °C for all three hydrous oxides, regardless of the difference in drying approach. The microwave-dried and conventional IR heating dried hydroxide powders exhibit very similar thermal losses when heated at 10 °C min^{-1}. In comparison, the organic solvent dehydrated hydroxide powder exhibits a 3%–4% lower weight loss than either the microwave-dried powder or the conventional IR heating dried hydroxide powder. These TGA results imply that organic solvent dehydration is a more effective

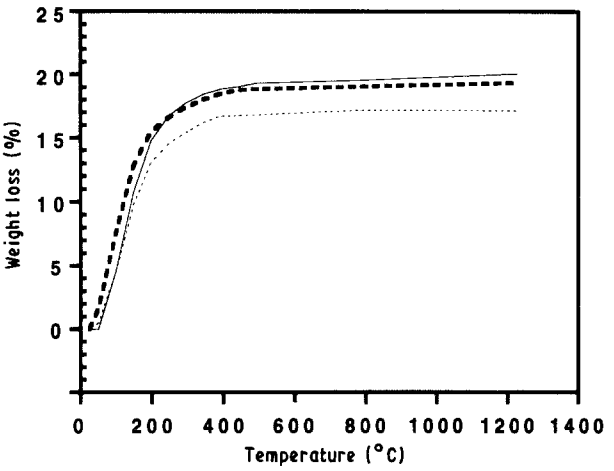

Figure 9 TGA traces for the hydrous oxides processed via (– – –) organic solvent dehydration, (- - -)microwave drying, and (——) conventional heating drying routes.

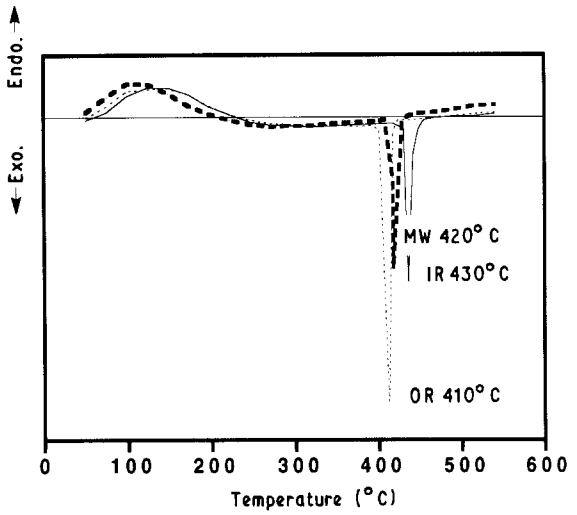

Figure 10 DTA traces for the same materials shown in Fig. 9. The crystallization of $Hf_{0.25}Zr_{0.75}O_2$ powder particles occurred immediately after the dehydration process was completed.

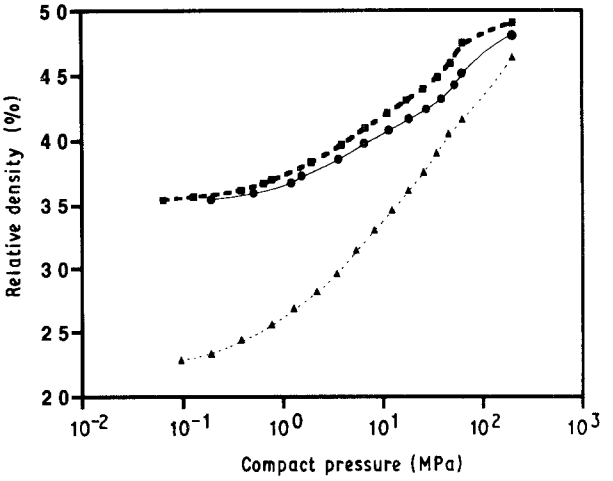

Figure 11 The compacted density as a function of compaction pressure for the oxide powders processed via (▲) organic solvent dehydration, (■) microwave drying, and (●) conventional heating drying routes.

dehydration process than either microwave drying or conventional IR heating drying. Fig. 10 also shows that crystallization of amorphous $Hf_{0.25}Zr_{0.75}O_2$ particles occurred almost immediately after the dehydration process was completed. The drying route had little impact on the crystallization temperature of the fully dehydrated $Hf_{0.25}Zr_{0.75}O_2$ powders. The crystallization temperature is 410, 420 and 430°C for the powders processed from the hydroxides dried via the OR, MW and IR routes, respectively.

Fig. 11 and Table III show the tap and compacted green densities as a function of uniaxial compaction pressure for the powders processed via the three different drying approaches. The organic solvent dehydrated oxide powder has a much lower tap density than either the microwave-dried oxide powder or the conventional IR heating lamp-dried oxide powder. The compacted density of the organic solvent dehydrated oxide powder is also much lower than that of either the microwave-dried oxide powder or the conventional IR heating lamp-dried oxide powder when the compaction pressure is below 100 MPa. With increasing compaction pressure over the pressure range 1–100 MPa, the compacted density of the organic solvent dehydrated oxide powder increases dramatically. At 100 MPa, the three oxide powders exhibit similar compacted densities, although the microwave-dried oxide powder compact is slightly denser than the other two. It is known that the green density of a ceramic powder compact is largely dependent on the characteristics of the powder, such as crystallite size, particle size, particle-size distribution and, in particular, the degree of particle agglomeration [18, 19]. For example, a highly crystallized ceramic powder exhibits a higher compacted density than a finely divided or an amorphous ceramic powder at a given compaction pressure. The presence of hard agglomerates or aggregates in a ceramic powder has a strong influence on the pressure dependence of compacted density. As was discussed above, the average particle/aggregate size of the organic solvent

TABLE III The tap density, compacted green density, and the agglomerate strength for the oxide powders processed via three different drying routes

	Drying route		
	OR	MW	IR
TAP density (% theoretical)	26.3	37.5	36.8
Green density (% theoretical) (at 100 MPa)	46.4	49.0	48.4
Agglomerate strength (MPa)		40	40

dehydrated oxide powder is smaller than that of either the microwave dried or conventional heating lamp dried oxide powders. More importantly, the packing density of primary particles within powder agglomerates in the former is lower than that in the latter two. Its tap and compacted densities are thus lower than those in either the microwave-dried or conventional heating dried oxide powders. It is estimated from the pressure dependence of compacted density that the compaction strength of powder agglomerates is approximately 40 MPa in both the microwave-dried and conventional heating dried oxide powders.

A preliminary study has been made of the sinterability of these three oxide powders processed via different drying routes by sintering the powder compacts at temperatures in the range 1300–1400°C. Table IV shows the sintered density at 1300°C for 2 h for the oxide powders processed via the OR, MW and IR routes, respectively. The conventional heating lamp-dried powder compact exhibited an unsintered powder-like structure on sintering at 1300°C for 2 h. This indicates that little densification occurred in this material at the sintering temperature. Similarly, the microwave-dried oxide powder compact was not properly sintered, although its sintered density is slightly higher than that for the conventional heating lamp-dried powder compact. By comparison, the organic

TABLE IV The sintered density at 1300 °C for 2 h for the oxide powders processed via the three different drying routes

Drying route	Sintered density (% theoretical)
OR	84.8
MW	63.4
IR	56.6

solvent dehydrated oxide powder compact exhibited a sintered density of 84.8% theoretical on sintering at 1300 °C for 2 h. Both the microwave-dried and conventional IR heating lamp-dried oxide compacts showed an unsintered powder structure on sintering at 1400 °C for 2 h. The organic solvent dehydrated oxide compact was, however, seriously cracked on cooling from 1400 °C. As was confirmed by XRD phase analysis, the spontaneous tetragonal to monoclinic transformation had occurred on cooling from the sintering temperature in this sample. The volume expansion and shear deformation associated with the transformation resulted in the formation of a crack network. It was estimated that the sintered density of this material was above 90% theoretical.

4. Conclusions

Co-precipitation of mixed zirconium and hafnium oxynitrates in an ammonia solution of pH 10.5 results in the formation of amorphous zirconium–hafnium hydroxide, which forms monoclinic $Hf_{0.25}Zr_{0.75}O_2$ on calcining at 600 °C for 4 h. The characteristics of the calcined and then ball-milled oxide powder, such as particle/aggregate size, particle/aggregate-size distribution, particle/aggregate morphology, and the degree of particle agglomeration, are influenced strongly by the drying route by which the co-precipitated hydrous oxide gels are dried. The oxide powder processed from the hydroxide dried via the organic solvent dehydration route exhibits smaller average particle/aggregate size and a much lower degree of powder agglomeration than the oxide powders processed from the hydroxides dried via either the microwave drying route or the conventional heating lamp drying route. It has been shown that the occurrence of hard particle aggregates in the calcined oxide powders is due to a high degree of particle agglomeration in the as-dried hydroxide powders. The fine particle/aggregate size and in particular the low degree of powder agglomeration in the $Hf_{0.25}Zr_{0.75}O_2$ powder processed via the organic solvent dehydration route lead to a high sinterability and a low sintering temperature.

Acknowledgement

J. Wang thanks the SERC for financial support during the period when the work was carried out.

References

1. R. C. GARVIE, R. H. J. HANNINK and R. T. PASCOE, *Nature* **258** (1975) 703.
2. N. CLAUSSEN, *Mater. Sci. Engng.* **71**, (1985) 23.
3. N. CLAUSSEN, M. RUHLE and A. H. HEUER (eds), "Advances in Ceramics", Vol. 12, "Science and Technology of Zirconia II" (The American Ceramic Society, Columbus, OH, 1984).
4. J. WANG, H. P. LI and R. STEVENS, *J. Mater. Sci.* **27** (1992) in press.
5. T. Y. TIEN, T. K. BROG and A. K. LI, *Int. J. High. Tech. Ceram.* **2** (1986) 207.
6. O. HUNTER Jr, R. W. SCHEIDECKER and S. TOJO, *Ceram Int.* **5** (1979) 137.
7. J. E. BAILEY, D. LEWIS, Z. M. LIBRANT and L. J. PORTER, *J. Brit. Ceram. Soc.* **71** (1972) 25.
8. R. RUH, H. J. GARRETT, R. F. DOMAGALA and N. M. T ALLAN, *J. Amer. Ceram. Soc.* **51** (1968) 23.
9. G. W. KRIECHBAUM, P. KLEINSCHMIT and D. PEUCKERT, *Ceram. Trans.* **1** (1988) 146.
10. S. L. DOLE, R. W. SCHEIDECKER, L. E. SHIERS, M. F. BERARD and O. HUNTER Jr, *Mater. Sci. Engng.* **32** (1978) 277.
11. W. H. RHODES, *J. Amer. Ceram. Soc.* **64** (1981) 19.
12. D. W. JOHNSON and F. J. SCHNETTLER, *ibid.* **53** (1970) 440.
13. I. J. CHABINSKY and E. E. EVES III, *Ceram. Engng Sci. Proc.* **6** (1985) 1412.
14. D. W. LYONS, J. D. HATCHER and J. E. SUNDERLAND, *Int. J. Heat Mass Transfer* **15** (1972) 897.
15. M. S. KALISZEWSKI and A. H. HEUER, *J. Amer. Ceram. Soc.* **73** (1990) 1504.
16. S. L. JONES and C. J. NORMAN, *ibid.* **71** (1988) C-190.
17. L. M. TAU, R. SRINIVASAN, R. J. DE ANGELIS, T. PINDER and B. H. DAVIS, *J. Mater. Res.* **3** (1988) 561.
18. K. KENDALL, *Powder Metall.* **31** (1988) 28.
19. J. S. REED, and R. B. RUNK, in "Treatise on Materials Science and Technology", Vol. 9, "Ceramic Fabrication Processes", edited by F. F. Y. Wang (Academic Press, New York, 1976) p. 71.

Received 6 April
and accepted 2 June 1992